

Status Report (22th J-PARC PAC): Searching for a Sterile Neutrino at J-PARC MLF (E56, JSNS²)

October 27, 2016

M. Harada, S. Hasegawa, Y. Kasugai, S. Meigo, K. Sakai,
S. Sakamoto, K. Suzuya
JAEA, Tokai, JAPAN

T. Maruyama¹, S. Monjushiro, K. Nishikawa, M. Taira
KEK, Tsukuba, JAPAN

S. Iwata, T. Kawasaki
Department of Physics, Kitasato University, JAPAN

M. Niiyama
Department of Physics, Kyoto University, JAPAN

S. Ajimura, T. Hiraiwa, T. Nakano, M. Nomachi, T. Shima, Y. Sugaya
RCNP, Osaka University, JAPAN

T. J. C. Bezerra, E. Chauveau, H. Furuta, Y. Hino, F. Suekane
Research Center for Neutrino Science, Tohoku University, JAPAN

I. Stancu
University of Alabama, Tuscaloosa, AL 35487, USA

M. Yeh
Brookhaven National Laboratory, Upton, NY 11973-5000, USA

W. Toki
Colorado State University, Fort Collins, Colorado, USA

H. Ray
University of Florida, Gainesville, FL 32611, USA

G. T. Garvey, C. Mauger, W. C. Louis, G. B. Mills, R. Van de Water
Los Alamos National Laboratory, Los Alamos, NM 87545, USA

E. Iwai, J. Jordan, J. Spitz
University of Michigan, Ann Arbor, MI 48109, USA

¹Spokesperson: (takasumi.maruyama@kek.jp)

Contents

1	Introduction	2
2	Timescale and Cost estimation for Detector Construction	3
3	Status of Studies for the TDR	3
3.1	Liquid Scintillator	3
3.1.1	Effect of Noise on PSD capability	4
3.1.2	New PSD Results using DIN-based Liquid Scintillator	7
3.1.3	Properties of Diluted Liquid Scintillator, PSD + Cherenkov	8
3.2	Veto System Design	10
3.2.1	Hardware Design Study	14
3.2.2	An Alternative Option for the Veto	15
3.3	Software / Simulation	15
3.3.1	The Reactor Analysis Tool (RAT)	15
3.3.2	Reproducing Data from the KEK Test Stand	16
4	MLF 2015AU0001 Test-Experiment	17
5	Summary	18

1 Introduction

The JSNS² (J-PARC E56) experiment aims to search for a sterile neutrino at the J-PARC Materials and Life Sciences Experimental Facility (MLF). After the submission of a proposal [1] to the J-PARC PAC, Stage-1 approval was granted to the JSNS² experiment on April 2015. This approval followed a series of background measurements which were performed in 2014 [2, 3].

Recently, funding (the grant-in-aid for scientific research (S)) in Japan for building one 25 ton fiducial volume detector module was approved for the experiment. Therefore, we aim to start the experiment with one detector in JFY2018-2019. We are now working to produce precise cost estimates and schedule for construction, noting that most of the detector components can be produced within one year from the date of order. This will be reported at the next PAC meeting.

In parallel to the detector construction schedule, JSNS² will submit a Technical Design report (TDR) to obtain the Stage-2 approval from the J-PARC PAC. The recent progress of the R&D efforts towards this TDR are shown in this report. In particular, the R&D status of the liquid scintillator, cosmic ray veto system, and software are shown.

We have performed a test-experiment using 1.6 L of liquid scintillator at the 3rd floor of the MLF building in order to determine the identities of non-neutrino background particles coming to this detector location during the proton bunch. This is the so-called

“MLF 2015AU0001” experiment. We briefly show preliminary results from this test-experiment.

2 Timescale and Cost estimation for Detector Construction

The following detector elements are considered for developing the JSNS² experiment.

- A stainless tank and an acrylic tank
- PMTs
- Liquid scintillator
- Veto system
- Electronics
- Slow components such as HV, slow monitors, and safety equipment.

The stress calculation for the stainless tank was done and submitted to the PAC already. We use 8” PMTs instead of 10” PMTs in order to optimize for the dynamic range of the PMT and electronics, however the oil (liquid scintillator) protection mechanism for the breeder chain is the same as for Double-Chooz and RENO [4]. The tapered breeder system to expand the non-saturation region between the input light yield and the output signal was tested and discussed in the status report [6]. A brief discussion of the cosmic ray veto system is presented later in this status report.

The other items involve finalizing the cost estimation and production time scale. The TDR will describe not only the design of these sub-systems, but also the relevant contracts and time-scale.

3 Status of Studies for the TDR

3.1 Liquid Scintillator

One of the most important goals of the JSNS² R&D is to produce a detector that is able to efficiently and purely discriminate fast neutron background events from signal events. One technique for distinguishing these signals is called Pulse Shape Discrimination (PSD), which takes advantage of the different timing characteristics of signal and background. The definition of the PSD variable is shown in the Fig. 1. As seen in the conceptual plot, the neutron background events have wider waveforms than that of signal events.

The other technique for distinguishing between signal and background is to use Cherenkov photons. An oscillated electron antineutrino IBD event is characterized by a final state positron, which emits Cherenkov light. However, neutron-induced proton events do not emit Cherenkov light at these low energies.

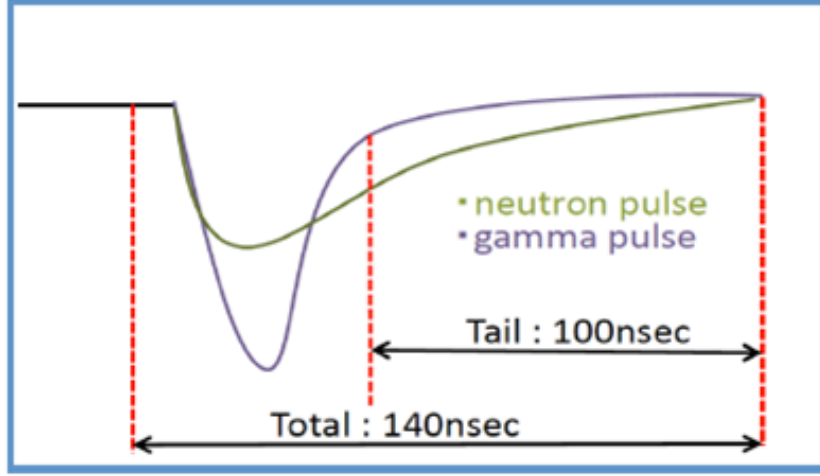


Figure 1: The PSD variable concept. Neutron background events have wider pulse shape than that of gamma / positron events. The PSD variable is defined as $\text{tailQ}/\text{totalQ}$ (where Q is charge).

The JSNS² progress on liquid scintillator R&D has been shown elsewhere [5, 6], therefore we only show the most relevant recent results.

3.1.1 Effect of Noise on PSD capability

In a previous status report [6], the estimated PSD capability of a full JSNS² detector with Daya Bay type Gd-loaded liquid scintillator (DBLS) was shown. This work was based on a MC study with neutrinos (signal) and cosmic-induced fast neutron samples after applying the neutrino selection criteria. However, the noise effect of the PMTs was not considered in the study at that time. Scintillation light in the JSNS² detector is viewed by a few hundred PMTs, and the PSD capability is evaluated with sum of the waveforms of all the PMTs. Compared with detecting the light using one PMT, the noise can affect the PSD capability considerably. Therefore, it is important for a more realistic PSD study in consideration of PMT noise. The PSD capability in the previous status report was recalculated implementing measured noise data with an 8 inch PMT (Hamamatsu R5912). Figure 2 shows an example of the measured noise waveform at Tohoku University. Figure 3 shows an example of waveforms from one PMT (the left figure) and the sum of the waveforms of all PMTs (the right figure) for the neutrino MC samples before and after including the noise data.

Two noise cases were considered, independent noise for each PMT (normal noise) and same noise for all PMTs (coherent noise) for the extreme case. Figures 4, 5 and 6 show the PSD distributions of the previous study, the normal noise case, and the coherent noise case, respectively.

The PSD distribution of the normal noise case is not changed so much comparing the previous result. However, the PSD distribution of the coherent noise indicates that the coherent noise affects the PSD capability more than the normal noise case. The coherent noise could be made inside electronics for data taking. It is necessary that the coherent noise is considered in the development of the electronics for JSNS². More quantitative analysis of the noise effect will be done in the near future.

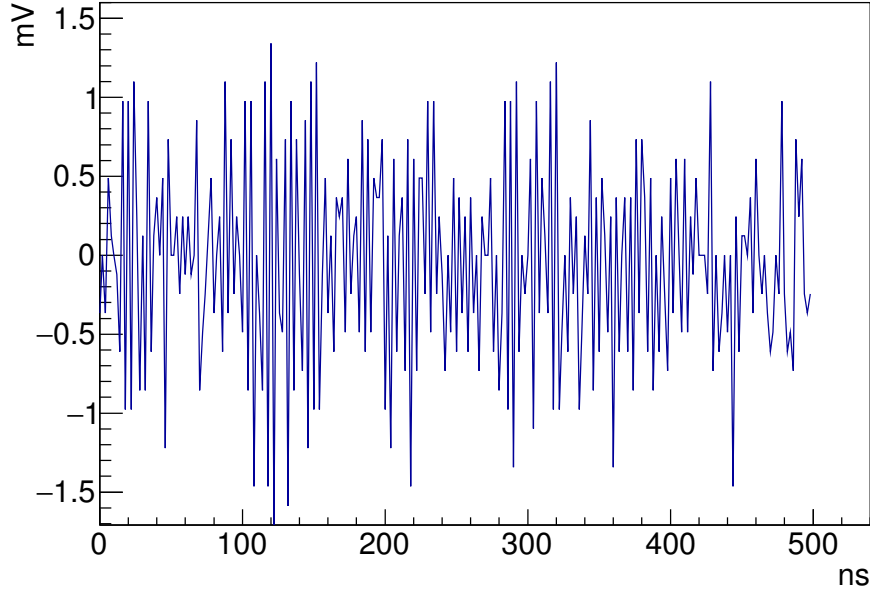


Figure 2: An example of the measured noise waveform with an 8 inch PMT at Tohoku University.

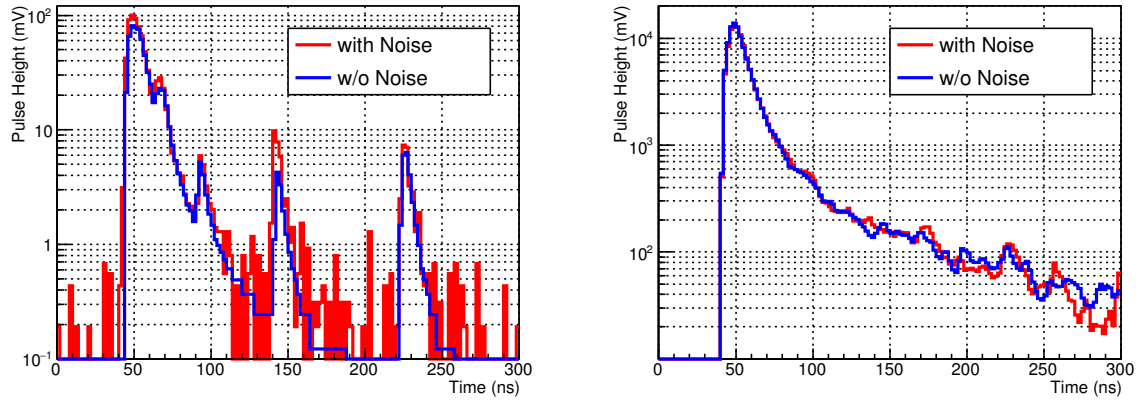


Figure 3: An example of a waveform from one PMT (left plot, 51 p.e.s) and the sum of the waveforms from all PMTs (right plot, 9200 p.e.s, 45MeV) in the neutrino MC samples. Blue and red lines show cases of with and without the noise data, respectively.

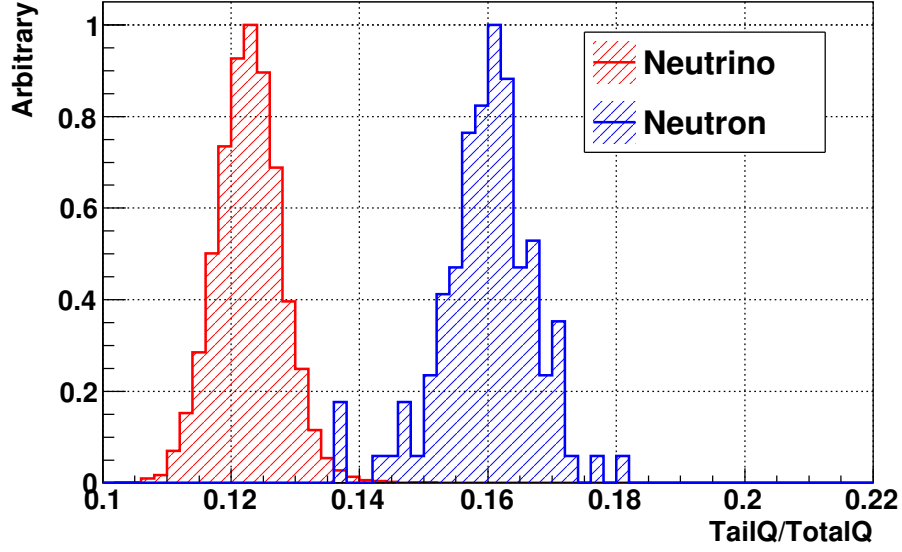


Figure 4: PSD distributions of the neutrino MC samples (red line) and the cosmic-induced fast neutrons (blue line, recoiled protons) in the previous status report.

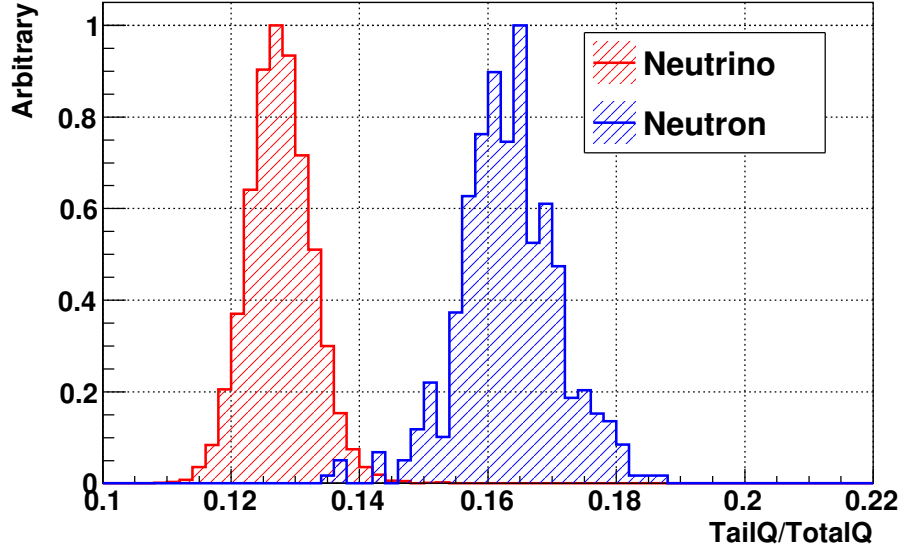


Figure 5: PSD distributions of the neutrino MC samples and the cosmic-induced fast neutrons (recoiled protons) after including the normal noise.

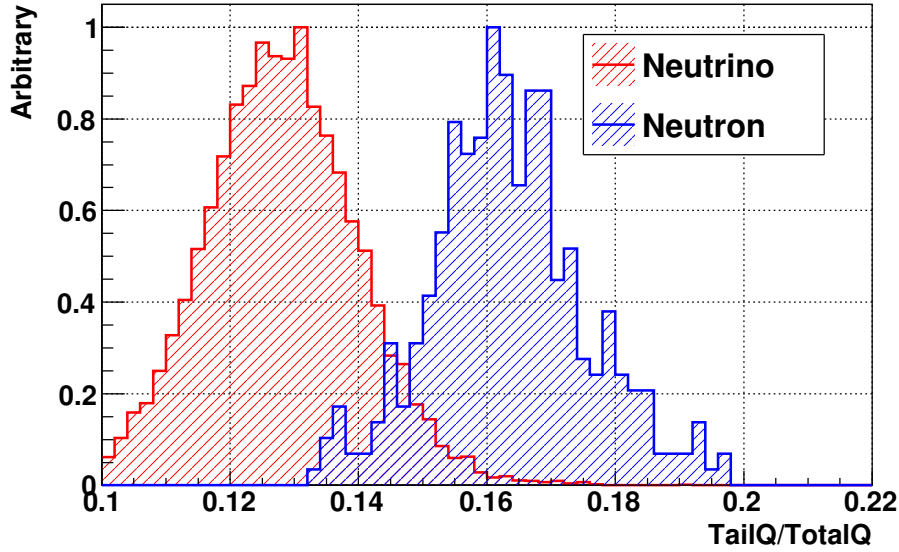


Figure 6: PSD distributions of the neutrino MC samples and the cosmic-induced fast neutrons (recoiled protons) after including the coherent noise.

3.1.2 New PSD Results using DIN-based Liquid Scintillator

In this subsection, we show new PSD results using DIN-based liquid scintillator.

A schematic diagram of the test stand used to evaluate the scintillator mixtures is shown in Fig. 7. A Cf-252 source was placed near a piece of plastic scintillator with a PMT (Hamamatsu H6410) viewing it. Another PMT (Hamamatsu H6559) was placed approximately 130 cm away looking at the liquid scintillator sample being tested. In these tests, we used an LAB-based scintillator cocktail (LAB + 3.0 g/L PPO + 15 mg/L bis-MSB) and a DIN-based scintillator cocktail (DIN + 3.0 g/L PPO + 15 mg/L bis-MSB) provided by BNL. Both scintillator cocktails were bubbled with nitrogen for 1 hour to remove impurities that quench scintillation light. We looked for coincident hits in both the plastic and liquid scintillators to identify Cf decays. Signals were read out using a 14-bit CAEN DT5730 digitizer at 500 MS/s.

To determine if an event in the liquid scintillator was a neutron or a gamma, we used time of flight (TOF) information. By measuring the time difference between the triggers in the liquid and plastic scintillators it was possible to tell if an event was a gamma (short TOF) or a neutron (long TOF). Histograms of the time of flight distributions for two different scintillator cocktails are shown in Fig. 8.

We can exploit the fact that neutron and gamma waveforms have different shapes (see average waveforms in Fig. 9) to define a pulse shape discrimination variable which is simply the amount of charge in the tail divided by the total charge in the whole waveform, often denoted Tail Q / Total Q. Neutrons have long tails and thus will generally have higher values of Tail Q / Total Q than gamma events. This fact will allow us to distinguish between the two types of events and reject fast neutrons.

One prominent background to this measurement is misclassified gammas that are counted as neutrons due to accidental coincidence between two consecutive Cf decays. We already subtracted the effects using offline information to estimate the rejection factor

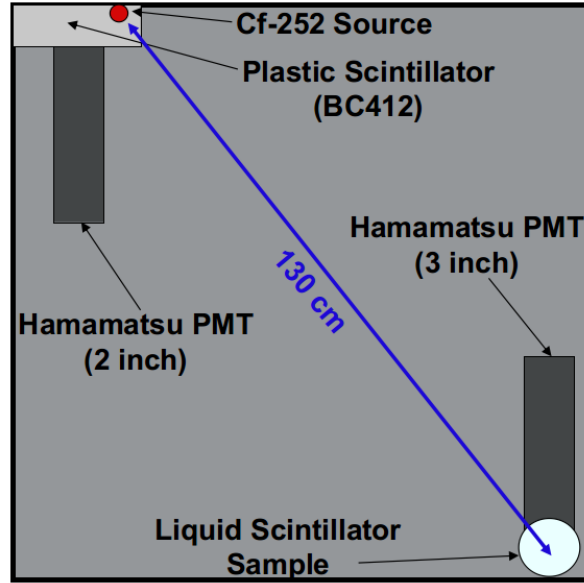


Figure 7: Schematic diagram of the dark box used for our scintillator tests. PMTs and scintillators not shown to scale.

of the neutron events and the detection efficiency of the gamma events.

In Fig. 10, the gamma and neutron distributions are shown side by side with the misclassified gamma events removed. It is this background-subtracted data that will be used to quantify the neutron rejection factor and gamma detection efficiency.

For this analysis, only events with between 200 and 800 photoelectrons (PEs) were used to assess the pulse shape discrimination performance of the scintillator cocktails. This population was chosen to include the highest energy neutron events (~ 10 MeV neutrons), but also to get sufficient statistics for background measurements.

Using these events, we were able to achieve a neutron rejection factor of 100 with a gamma detection efficiency of 73.1% for the LAB-based scintillator and 99.5% with the DIN-based scintillator. With high energy events and better photocoverage in the full detector, these values will improve. We can also pair this pulse shape discrimination technique with Cerenkov light timing to get even better neutron rejection factors.

3.1.3 Properties of Diluted Liquid Scintillator, PSD + Cherenkov

At this PAC meeting, the concrete recipe to make the liquid scintillator is proposed to combine PSD and Cherenkov method in order to have strong rejection power of the neutron events induced by cosmic rays. The recipe is to use LAB (Linear alkylbenzene) + 0.5g/L PPO (secondary emission material).

Dr. Furuta (Tohoku University) found that the emission time constant of the scintillation light depends on the concentration (density) of the secondary light emission materials such as PPO or b-PBD. Using different concentrations of this material provides not only different scintillation light yields but also different emission time constants. Figure 11 shows the dependence of the PPO concentration on the light yield and the emission time constant. The emission time of scintillation light is getting slower as the concentration is decreased. This means that lower PPO concentration gives better condition for the Cherenkov method, while PSD capability is better in the higher concentration condition.

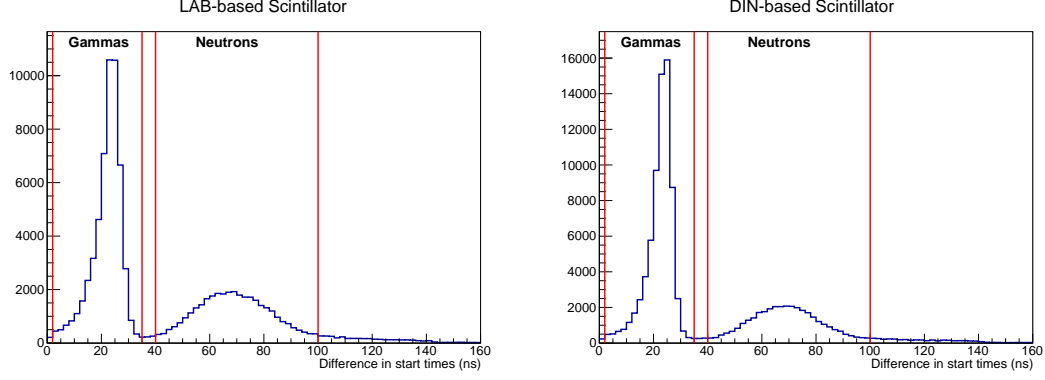


Figure 8: Time of flight for events in the LAB-based scintillator (left) and the DIN-based scintillator (right). The population at low time of flight values is gammas and the population with longer time of flight values contains neutrons. The red lines mark the boundaries of the regions used to classify events as gammas and neutrons.

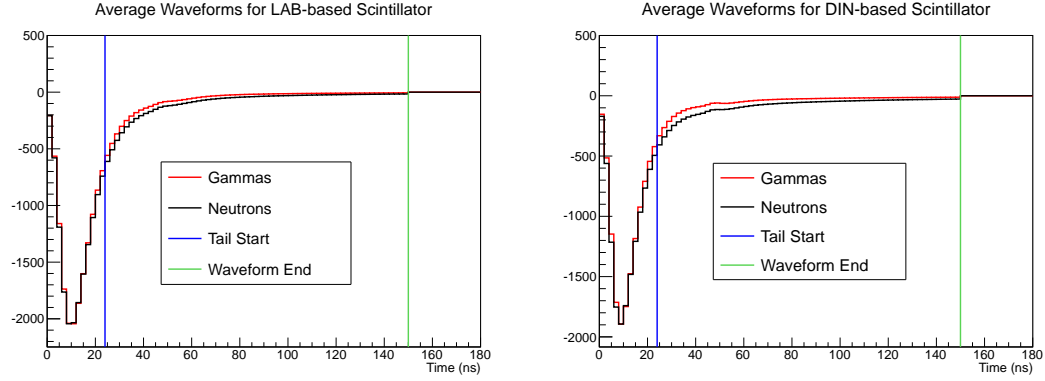


Figure 9: Average waveforms for neutrons (black) and gammas (red) in the LAB-based scintillator (left) and the DIN-based scintillator (right). The neutron waveforms show a longer tail in both scintillator cocktails. We define the tail as the portion of the waveform after the blue line.

The pulse shape difference between gamma ray events and neutron events measured by a vial size detector with Cf source is shown in Fig. 12. The black line shows the gamma events, while the red line shows the neutron events. The horizontal axis corresponds to the TDC counts, corresponding to 2ns / count. After 80 counts (~ 160 ns), there are remarkable pulse shape differences. The difference is smaller than a normal PPO 3.0 g/L case, but the difference still exists. The preliminary study for the PSD method using likelihood gives good identifications between gamma and neutron events even in this condition.

The Cherenkov light yield compared to the scintillation light yield is measured by KEK teststand [5]. The analysis method is identical to those used in the reference. All photons coming to the 2" PMT are at one photo-electron level because the mean light yield is about 0.4 p.e. Figure 13 shows the results. The horizontal axis shows the relative light emission timing with respect to the muon passing timing. We still see the Cherenkov component in the fastest timing bin, but the light yield ratio between the Cherenkov component vs. scintillation light is almost one even in the fastest timing bin.

Using these results, we can estimate the rejection power of fast neutron events using a

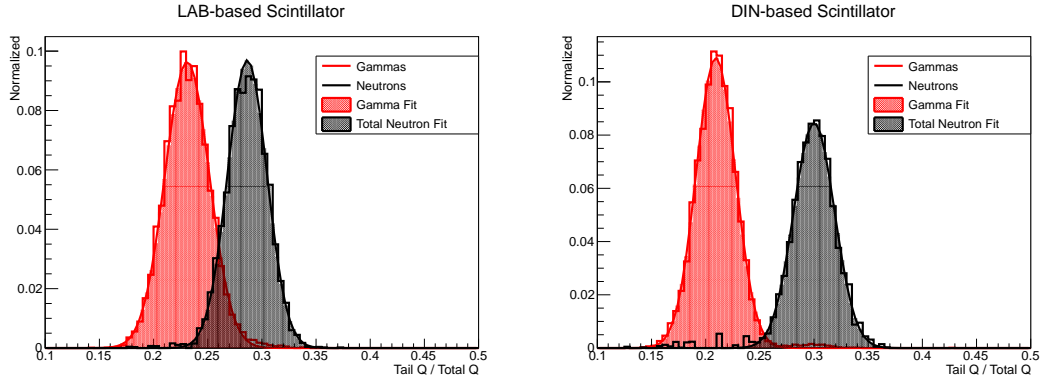


Figure 10: Measured distributions of Tail Q/Total Q for neutron (black histogram) and gamma events (red histogram) in the LAB-based scintillator (left) and the DIN-based scintillator (right). Misclassified gammas in the neutron population have been removed. Fits to the neutron and gamma distributions are shown as the filled Gaussians.

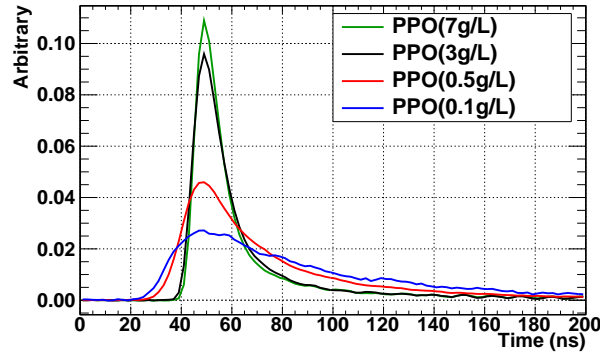


Figure 11: PPO concentration dependence of the mean waveform. It is clear that the concentration affects not only light yield but also the light emission constant.

simulation of the real JSNS² detector. Note that this result set the PMTs apart from the light source by ~ 70 cm. If the vertices are farther than 70 cm, the situation is improved because the number of scintillation photons is reduced by $1/r^2$, where r is the distance between light source and a PMT, while the number of Cherenkov photons are reduced by $1/r$ due to the ring image. For example, the ratio of Cherenkov and scintillation light in the fastest timing bin is more than 10 times better in the case that the vertex is located at the center of the detector ($r \sim 280$ cm).

3.2 Veto System Design

As shown in Fig. 14, in the current detector design, the fiducial target region filled with Gd-loaded liquid scintillator and the buffer liquid scintillator layer are surrounded with an additional liquid scintillator layer to veto mainly charged particle from the outside.

In the previous status report [2] for the 19th J-PARC PAC, the veto layer was used to suppress the delayed backgrounds coming from beam neutrons coming on the proton

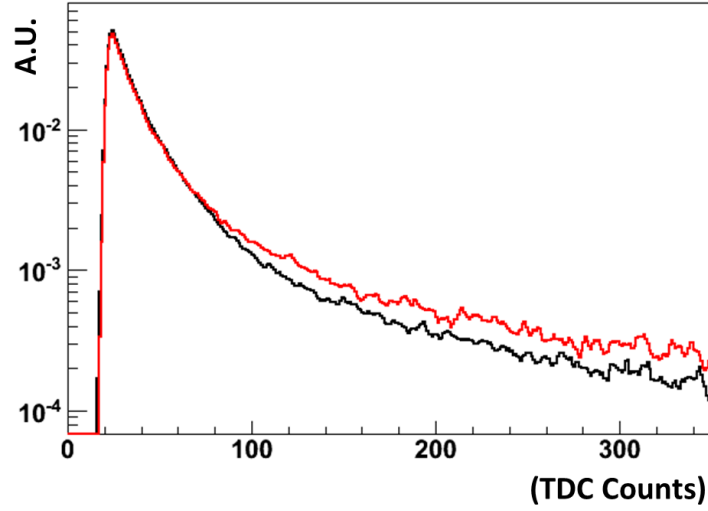


Figure 12: The pulse shape difference between gamma events and neutron events measured by a vial size detector using a Cf radioactive source. The black line shows the gamma events, while the red line shows the neutron events. The horizontal axis corresponds to the TDC counts, which provides 2ns / count. Later than the 80 counts (~ 160 ns), there are remarkable differences in pulse shape.

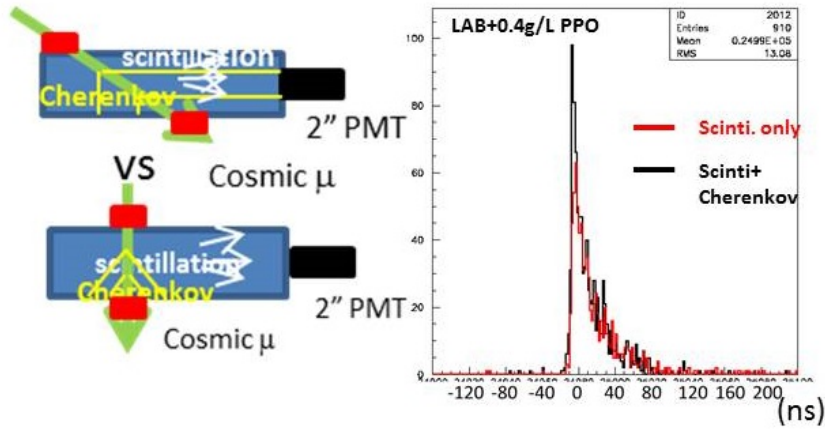


Figure 13: The Cherenkov light yield measurement using the KEK test-stand [5]. Using the two different setups shown in the left, the scintillation light timing and the scintillation timing + Cherenkov light timing was observed. Even in this condition, we can see the Cherenkov light in the fastest timing bin.

bunch timing. Some of the fast neutrons on the bunch timing are thermalized in the detector and captured by Gd to make delayed backgrounds (Fig. 14). Most of them produce some activity in coincidence with the bunch timing. The veto system helps to reject these backgrounds. In the previous study, the energy threshold to detect such activities was set to 0.5 MeV for both the central region and the veto layer.

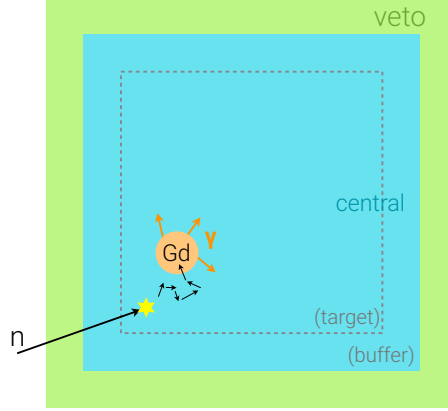


Figure 14: A schematic view of the JSNS² detector, and the delayed background induced by a fast neutron.

An energy threshold of 0.5 MeV is hard to utilize for the JSNS² detector because of the energy range of the environmental gammas (up to 2.6 MeV) and those of gammas from PMT glass, the acrylic vessel, and liquid scintillator. We thus study the case with a detector energy threshold of 3.0 MeV.

Figure 15 shows the energy deposit in the central region of the detector with the beam fast neutrons coming in coincidence with the proton bunch timing, which later make delayed background, obtained with a MC simulation. Note that this energy deposit does not include the quenching factor in the liquid scintillator, thus we will include it in the next publication. The assumed energy distribution and the flux of the beam fast neutrons are based on the measurement at the candidate detector location, and it is same as the previous study (described in the article [2]). In terms of the energy deposit distribution of the central region, there is no need to apply the energy threshold of 0.5 MeV, therefore 3.0 MeV is a reasonable threshold.

The energy deposit distribution in the veto layer in coincidence with the bunch timing for all of (black) and the remaining background after the central energy cut with 3.0 MeV (red) is shown in Fig. 16. An energy threshold of 3.0 MeV is good enough to keep a good rejection factor of the remaining background.

Although the quenching factor should be included to obtain the final number, more than 99% of the delayed background created from beam neutrons can be tagged with a 3.0 MeV energy threshold.

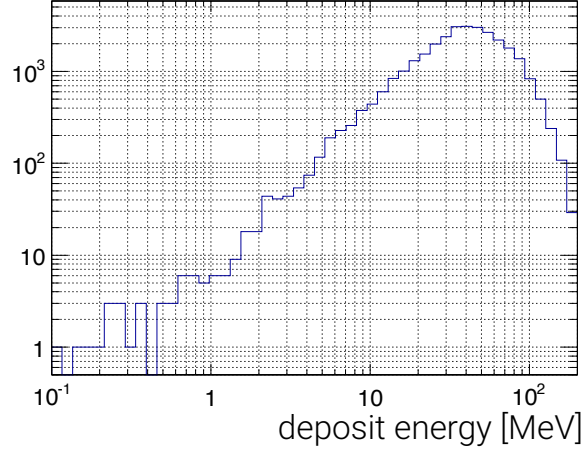


Figure 15: The true energy deposit in the central region with beam fast neutrons coming on the bunch timing, which later make delayed background, obtained with a MC simulation. Note that this does not include quenching factors inside the liquid scintillator.

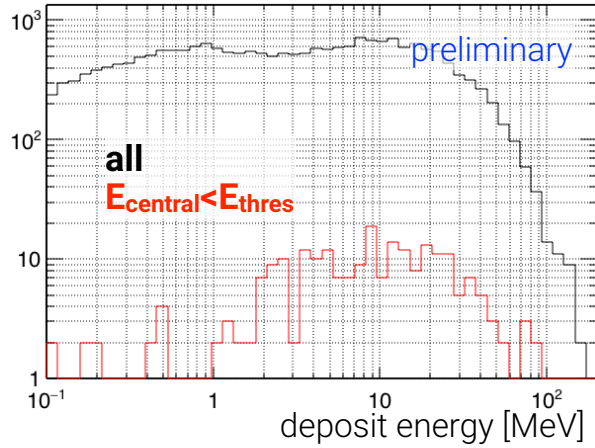


Figure 16: The energy deposit in the veto layer with beam fast neutrons coming on the bunch timing, which later make delayed backgrounds, obtained with a MC simulation. Black corresponds to all the activity, while the red shows the remaining background after the central energy cut. The energy threshold for the central region is 3 MeV. Note that this does not include quenching factors inside the liquid scintillator.

3.2.1 Hardware Design Study

The veto performance has been studied with a MC simulation. Figure 17 shows the tested setup. The veto layer (25 cm thick) surrounds the central region. The scintillation light from the veto layer is viewed by 50 5" PMTs (top and bottom: 10 each, side: 30). The inner and outer surfaces of the veto are covered by reflecting sheets. One candidate of the reflection sheet is called VM2000, which gives more than 97% reflectance for > 400 nm ($98.3\% @ 430\text{nm}$)[7]. We evaluated the expected light yield as a function of the reflectance of the reflection sheet. Figure 18 shows the result. The expected light yield is about 350 photoelectrons² for MIP particles (energy deposit of 40 MeV) with a 90% reflecting sheet; it is about 10 times of without the reflecting sheet.

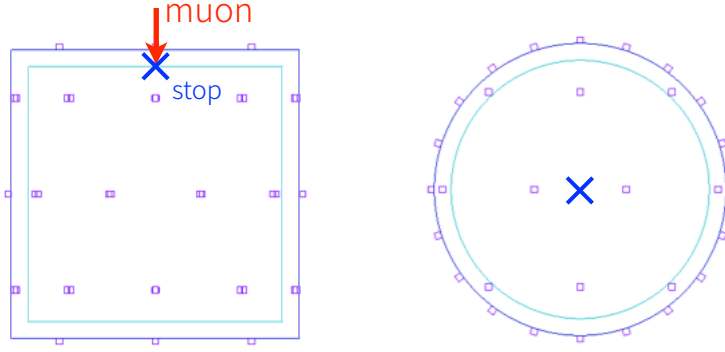


Figure 17: The MC setup for the veto performance evaluation. The inner and outer surfaces of the veto layer are covered by reflecting sheets and the layer is viewed by 50 5" PMTs.

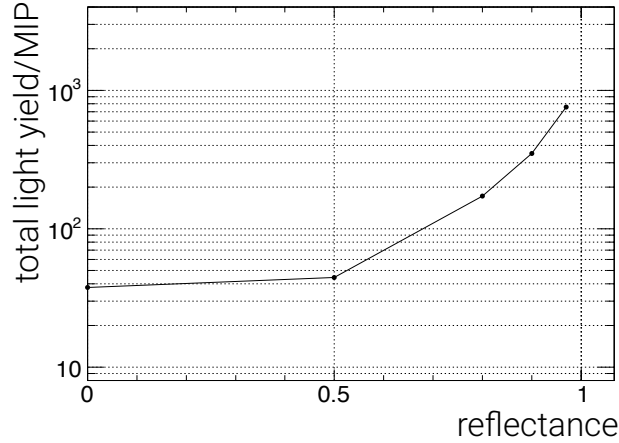


Figure 18: The expected total light yield for MIP particles as a function of the reflectance at the surface of the veto layer.

By using a high-reflection sheet to increase light-yield, light distribution was spread out over the whole veto layer, and some of the scintillation light can be detected even on the opposite side to the incident plane. The position resolution was thus also studied.

²Assuming 10000 photon/MeV for the liquid scintillator, and the relevant QE for the PMT

With the configuration described above, the position resolution is about 7.5 cm for MIP particles as shown in Fig. 19.

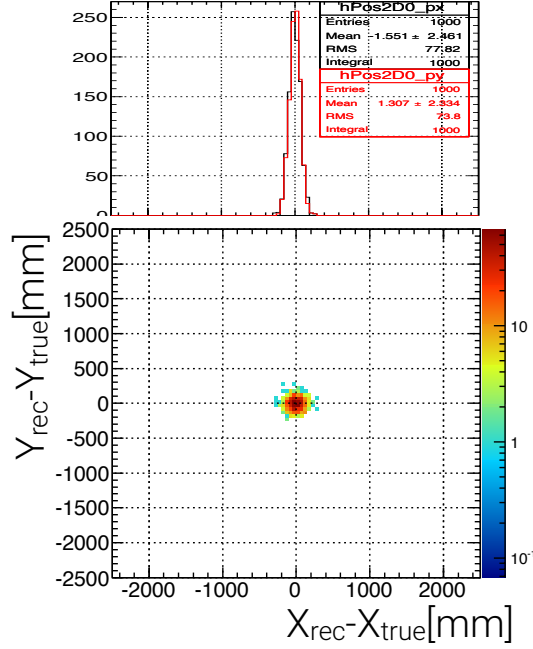


Figure 19: The residual distribution of the reconstructed positions.

3.2.2 An Alternative Option for the Veto

As mentioned in the status report in 2015 [5], we have an option to use SiPMs in the veto region. Here we assume to segment the veto layer with $30\text{cm} \times 30\text{cm}$ in order to have strong spatial resolution (~ 700 SiPMs are needed in this case). A preliminary study to use SiPMs ($12\text{mm} \times 12\text{mm}$) and a reflector with 90% reflectivity in all segmented area provides an acceptance of scintillation photons at 18 photons / MeV. This acceptance is good enough to detect the particles with a MeV.

3.3 Software / Simulation

3.3.1 The Reactor Analysis Tool (RAT)

The Reactor Analysis Tool (RAT) is a simulation framework which adds new physics lists to Geant4 [8]. In particular, RAT adds many features which allow for the detailed simulation of scintillation light. RAT makes it possible to input many of the most important parameters that characterize a scintillator including absorption length, refractive index, scintillation spectrum, and many more. With the ability to naturally specify all of these

parameters, it is possible to run more accurate simulations to characterize a detector and all relevant backgrounds.

3.3.2 Reproducing Data from the KEK Test Stand

It has been shown in previous status reports that the background rates in JSNS² are manageable if a neutron rejection factor of 100 can be achieved [2, 5]. Recoil protons in the 20-60 MeV range created by fast neutrons will not produce Cerenkov light and thus can be rejected using Cerenkov light timing. This technique was used successfully by LSND and needs to be independently verified for the scintillator under consideration for JSNS².

Measurements were done at KEK to quantify the fractions of Cerenkov and scintillation light in a dilute liquid scintillator cocktail. Scintillator paddles were used to select cosmic rays passing through a tube of liquid scintillator (1 m in length, 13 cm diameter) in two different configurations. These two configurations are shown in Fig. 20. In the scintillation only configuration, muons pass straight through the detector so that no Cerenkov light reaches the PMT at the end of the scintillator tube. In the scintillation + Cerenkov configuration, the muon tracks enter the scintillator at an angle so that some of the Cerenkov light will reach the PMT. More details can be found in previous status reports which contain the test results [5, 6].

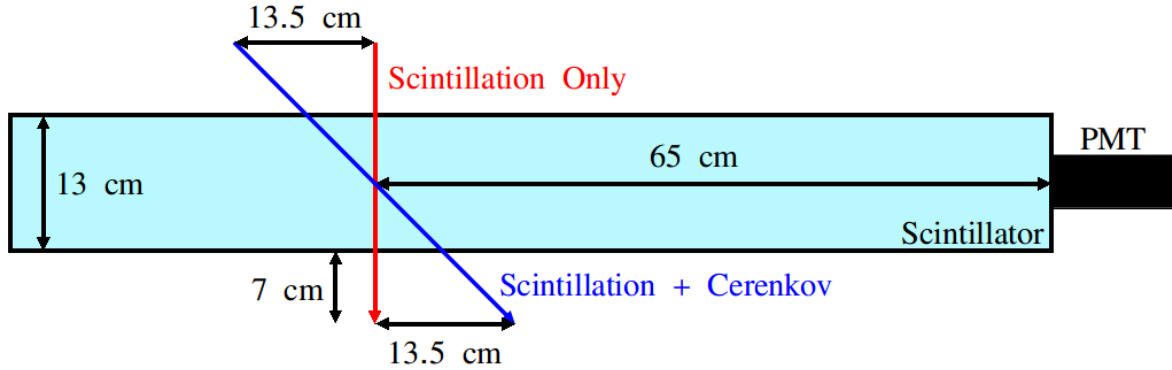


Figure 20: A schematic diagram of the KEK test stand geometry used in RAT. The red path represents 4 GeV muons in the scintillation only configuration and the blue path represents 4 GeV muons in the scintillation + Cerenkov configuration.

We are interested in replicating the measurements from the KEK test stand using RAT to verify that the simulation is working correctly and to ensure that we can reproduce the scintillator behavior in simulation. The geometry shown in Fig. 20 was constructed in RAT and 4 GeV muons were simulated through the two paths shown. The scintillation time constants used in the simulation were taken from fits done to measurements made at the KEK test stand in the scintillation only configuration. This fit is shown as the red line in Fig. 21. Since the scintillator used in the KEK test stand was dilute (0.5 g/L PPO as opposed to 3.0 g/L PPO for DBLS), the light yield was changed from 10,000 photons/MeV to 4,000 photons/MeV.

In order to control for the fact that there is more scintillation light in the scintillation + Cerenkov configuration than in the scintillation only configuration due to the longer

path length, the waveform tails (where there is no Cerenkov light) were used as a “side-band” to set the normalization. All bins to the right of the pink line in Fig. 21 were integrated and the two histograms were scaled so that these integrals would be equal.

The scintillation only data produced by RAT matches the scintillation only data taken at KEK. There is also a clear excess of Cerenkov light at early times that could be used to distinguish between different types of particles. This tendency is clearly similar to the Fig. 13 although more quantitative comparison will be performed. The ratio of Cerenkov to scintillation light at early times is highly dependent on the particle energy so a more realistic cosmic ray generator is being investigated to improve these results.

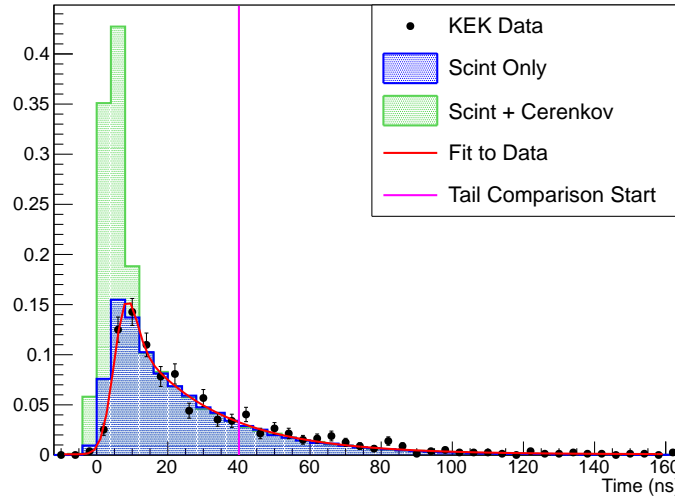


Figure 21: A comparison between RAT simulation results and KEK data in the scintillation only configuration (black points). The blue filled histogram is simulation data in the scintillation only configuration and the green filled histogram is data from the scintillation + Cerenkov configuration. The red line is a fit used to extract the time constants from the data. Bins to the right of the pink line were used to normalize the scintillation contributions to the simulation results.

4 MLF 2015AU0001 Test-Experiment

This test-experiment has been done from May to June in 2016 at the MLF 3rd floor³.

The goal of the experiment is to measure the PID of the background events, which occur in coincidence with the proton bunch timing, using 1.6 L of liquid scintillator. This liquid scintillator is good at separating neutrons from gamma events with PSD. We assumed all of this activities are coming from neutrons[2], but we may have a smaller number of delayed neutron background and a smaller neutrino oscillation signal detection efficiency in the case that there are a large number of gamma events. Therefore, this

³ Collaborators of this test experiment are followings; S.Meigo, S.Hasegawa (JAEA), E.Iwai, T.Maruyama (KEK), T.Hiraiwa, T.Shima (Osaka RCNP), H.Furuta, Y.Hino, F.Suekane (Tohoku), J.Spitz (U of Michigan).

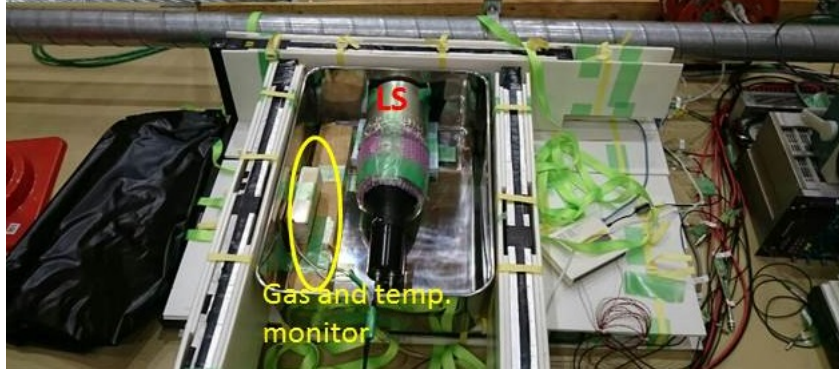


Figure 22: The setup of the 1.6L test measurement.

measurement is crucial for the real JSNS² experiment.

Figure 22 shows the setup of the experiment. This detector was put in a location similar to that of the current best candidate JSNS² detector location. The 1.6L LS detector was put inside a oil protection box made of stainless steel, and the box was surrounded by the veto counters made of plastic scintillator. Inside the box, there were temperature and gas level monitors to detect the liquid leak in the case of an emergency. This information was also monitored by those who in the MLF control room, and warning alarms were ready to alert operators in case of a liquid leak. Notably, it is envisioned that this system can be used for the real experimental case.

Figure 23 shows the preliminary results of the 1.6 L experiment. The horizontal axis shows the event timing, while the vertical axis corresponds to the energy of the events. Blue points show the neutron events without cosmic veto hits and red points show the hits of those of gamma rays. As can be seen in Fig. 23, gamma events are visible. The gamma events are mainly apparent in the faster timing region, as compared to the neutron events, with respect to the proton bunch timing. This is a good indication for the real JSNS² experiment because the number of delayed background events induced by beam neutrons should be reduced, and the time window of the prompt signal can be close to the proton event timing. Further quantitative statements will be shown in a publication in near future.

5 Summary

The most significant news for the JSNS² experiment is that the project received funding to construct the first of two 25 ton fiducial volume detector modules. We aim to start the JSNS² experiment in 2018-2019 with one detector. Currently, a concrete timescale and the budget of each experimental component is being estimated.

The studies for the TDR are also in good shape. Realistic MC simulation studies for the PSD capability using Daya-Bay type LS have been performed. In particular, it has been found that the effect due to noise is small if each channel is independent.

The primary candidate for the recipe to use both PSD and Cherenkov technique is LAB+0.5g/L PPO. The preliminary proto-type tests at Tohoku University and KEK

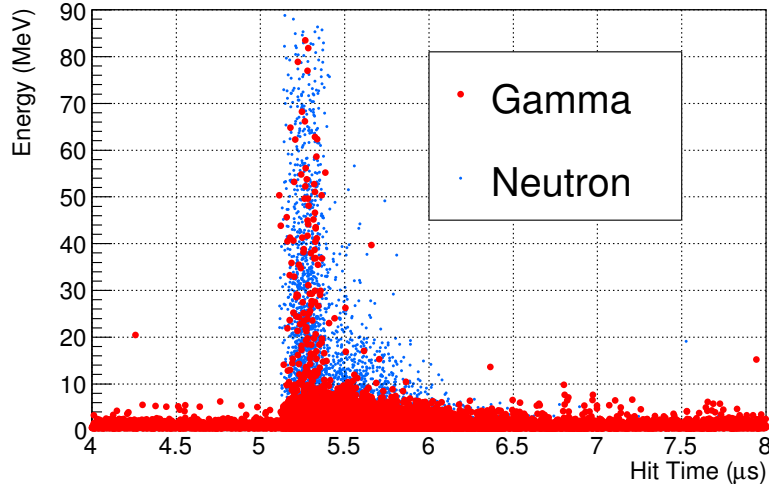


Figure 23: A preliminary result from the 1.6 L test measurement at the MLF. Blue points show the neutron events without cosmic veto hits and red points show gamma ray events. Horizontal axis shows the event timing, while the vertical axis corresponds to the energy of the events.

show that this recipe can provide both PSD and Cherenkov capabilities at the same time. We will determine the final recipe to make the liquid scintillator and present this in the upcoming TDR.

The veto design has been extensively discussed in this status report in order to demonstrate the ability to reject neutron and cosmic ray background events in the full JSNS² detector.

For the optical simulation, the RAT framework has been studied.

The test experiment, MLF 2015AU0001, has been performed from May-20 2016. This test aims to measure the identification of background particles arriving during or just after the MLF proton bunches. We have preliminary results, and will publish the paper soon.

References

- [1] M. Harada, *et al*, arXiv:1310.1437 [physics.ins-det]
- [2] M. Harada, *et al*, arXiv:1502.02255 [physics.ins-det]
- [3] S. Ajimura, *et al*, PTEP 2015 6, 063C01 (2015)
- [4] T.Matsubara, *et al.*, Nucl. Instrum. and Meth. A661 (2012) 16-25.
- [5] M. Harada, *et al*, arXiv:1507.07076 [physics.ins-det]
- [6] M. Harada, *et al*, arXiv:1601.01046 [physics.ins-det]

- [7] Private communication with Double Chooz collaboration.
- [8] <http://rat.readthedocs.io/en/latest/overview.html>.